Chinese Chemical Letters 34 (2023) 108031

Contents lists available at ScienceDirect

Chinese Chemical Letters

journal homepage: www.elsevier.com/locate/cclet

Thiol-ene crosslinked cellulose-based gel polymer electrolyte with good structural integrity for high cycling performance lithium-metal battery

Hongbing Zhang[a,1], Sijie Wang[a,1], Yujie Wang[a], Shuhan Dong[a], Wen Chen[a], De Li[a], Feng Yu[a,*], Yong Chen[b,*]

[a] State Key Laboratory of Marine Resource Utilization in South China Sea, Hainan Provincial Key Laboratory of Research on Utilization of Si-Zr-Ti Resources, Hainan University, Haikou 570228, China
[b] Guangdong Key Laboratory for Hydrogen Energy Technologies; School of Materials Science and Hydrogen Energy, Foshan University, Foshan 528000, China

ARTICLE INFO

Article history:
Received 21 October 2022
Revised 10 November 2022
Accepted 28 November 2022
Available online 5 December 2022

Keywords:
Gel polymer electrolytes
Cellulose
Crosslinked network
Thiol-ene click chemistry
Lithium-metal battery

ABSTRACT

Gel polymer electrolytes (GPEs) are considered to be one most promising alternative to liquid electrolytes due to their suitability for creating safe and durable solid-state lithium-metal batteries. However, the mechanical properties of GPEs usually deteriorate dramatically when polymer matrices are plasticized by a liquid electrolyte, which leads to significant loss of battery performance. Therefore, the long-term structural integrity and good mechanical strength are critical characteristics of GPEs designed for high-performance batteries. Here, an ecologically compatible cellulose-based GPE with a crosslinked structure is synthesized *via* a facile and effective thiol-ene click chemistry method. The prepared thiol-ene crosslinked GPE possesses enhanced mechanical strength (10.95 MPa) and rigid structure, which enabled us to fabricate $LiFePO_4$|Li batteries with ultra-long cycling performance. The capacity retention of the crosslinked cellulose-based GPE can be up to 84% at 0.5 C, even after 350 cycles, which is considerably higher than that of non-crosslinked GPE for which rapid decline in capacity occurs after 200 cycles. In addition, a GPE preparation method described in this work compares favorably well with existing commercial electrolytes for lithium metal batteries.

With progressive increases in the scale of global industrial production and consequent depletion of fossil fuel reserves, there is an urgent need for sources of clean and renewable energy. Lithium-metal batteries (LMBs) are considered to be one of the most promising electrochemical energy storage devices due to their high energy density (3860 mAh/g) and low redox potential (−3.04 V *vs.* standard hydrogen electrode) [1,2]. However, commercial carbonate-based liquid electrolytes used in LMBs raise safety concerns because of their flammability and cause dendrite growth on the lithium [3,4]. Unlimited growth of lithium dendrites due to uneven deposition of metallic lithium on the surface of the lithium metal anode during repeated charge/discharge cycles may result in short-circuit inside the battery [5,6].

Therefore, replacing the liquid electrolytes with solid polymer electrolytes (SPEs) is an effective solution to the indicated safety issues. The high mechanical strength and low dynamic mobility of SPEs can inhibit the growth of lithium dendrites [7–13]. But the frustrating ionic conductivity (lower than 10^{-3} S/cm) of SPEs at room temperature and their poor interfacial contact with the electrodes remain challenges to be overcome [14]. By contrast, gel polymer electrolytes (GPEs), which consist of a swollen polymer matrix plasticized with a liquid electrolyte, combine the advantages of both liquid and solid electrolytes and thus exhibit high ionic conductivity, good interfacial compatibility, and better safety performance [15,16]. Polyethylene oxide (PEO)-based GPEs have been widely utilized in LMBs due to their excellent electrolyte wettability, outstanding ability for coordination of lithium ions, and good flexibility [17–19]. However, commonly, the PEO-based GPEs contain plasticizers or solvents which inevitably reduce their mechanical strength and destabilize the structure [20–22]. For instance, Li *et al.* have prepared PEO-based gel polymer electrolytes with high ionic conductivity ($\sigma = 3.3 \times 10^{-3}$ S/cm) at room temperature [23], but Li/$LiFeO_4$ cells exhibited poor cycling stability at 0.5 C. Meanwhile, many other studies of non-crosslinked GPEs reported weak mechanical bonding inside, which in the long term

* Corresponding authors.
E-mail addresses: yuf@hainanu.edu.cn (F. Yu), ychen2002@163.com (Y. Chen).
[1] These authors contributed equally to this work.

https://doi.org/10.1016/j.cclet.2022.108031
1001-8417/

leads to degradation of the material due to repeated ion transport during charging and discharging [24].

Therefore, the design and synthesis of crosslinked GPEs with higher mechanical strength for use in LMBs attracts considerable interest. Thus, Li *et al*. developed polyhedral oligomeric silsesquioxane (POSS)-crosslinked poly(ethylene glycol) (PEG) composite electrolytes [25]. Li/Li symmetrical batteries with the GPEs exhibited a long service life of over 6800 h at a current density of 0.1 mA/cm^2. Zhang *et al.* fabricated novel crosslinked polymer electrolytes with excellent cycling stability at 1 C through a UV-initiated thiol-ene click reaction [26], but this GPE was supported on non-woven fabrics, and so the ionic conductivity of the prepared material at room temperature was relatively low (0.84×10^{-3} S/cm).

It is equally important to seek environmentally friendly renewable materials for high-strength GPEs with crosslinking networks and high ionic conductivity. As we know, most matrices of GPEs for lithium ion batteries consist of synthetic polymers such as PEO, PMMA, PVA and PVDF-HFP. Such polymer materials are expensive and can cause white pollution due to their non-degradability.

Cellulose is the most abundant natural biopolymer, which is derived from wood, algae and bacteria [27,28]. It displays good mechanical properties and good thermal and chemical stability due to strong intra- and intermolecular hydrogen bonds [29]. Cellulose is widely used as a binder, a polymer electrolyte, or a separator in batteries [30–33]. Zhou et al. successfully synthesized the novel bottlebrush *quasi*-solid-state polymer electrolyte BC-*g*-PLiSTFSI-*b*-PEGM through surface-initiated atom transfer radical polymerization and the prepared material displayed high mechanical strength and high ion conductivity [34]. However, other workers found that low uptake and retention of electrolytes is a common drawback of various cellulose-based GPEs [35]. At present, there are only few reports about crosslinked cellulose-based GPEs with superior electrolyte affinity and mechanical strength. Since pure cellulose is hydrophilic, this is not suitable for LMBs. Therefore, grafting PEG segment onto the cellulose backbone is an efficient way to improve the wettability of cellulose films by organic electrolytes and form cellulose organgels compatible with current LMB technologies.

Inspired by the above researches, we designed a facile and efficient thiol-ene click method to build crosslinked cellulose GPEs. First, cellulose is first chemically modified by allyl groups and then reacted with poly(ethylene glycol) methyl ether methacrylate (PEGMA) to obtain PEG-grafted cellulose (AP). Then, pentaerythritol tetra(3-mercaptoproponate) (PETMP) is used as a crosslinking agent to form crosslinked AP network. The as-prepared crosslinked AP and non-crosslinked AP dry films with a thickness of ~40–50 μm was cut into small wafers with a diameter of 14 mm and the mass of ~10 mg. Then these wafers were immersed in electrolyte solution to form gel polymer electrolytes (GPEs). The thickness of the GPE film was in the range of 120–150 μm. Compared to a non-crosslinked AP, the crosslinked AP can retain its stable structure and thus avoid infinite swelling and resulting collapse of its structure. Meanwhile, the crosslinked AP GPE exhibits the desirable values for ionic conductivity at room temperature and lithium-ion transport number. Moreover, $LiFePO_4$/Li batteries based on the crosslinked AP were demonstrated to have superior long-term cycling stability, which indicated that the structural strength and electrochemical performance were improved by the thiol-ene crosslinked network.

In previous work, we successfully synthesized non-crosslinked AP GPEs. These non-crosslinked AP GPEs were demonstrated to have good electrochemical properties and desirable cycling performance, which were achieved by controlling the degree of PEG grafting, and the prepared PEG-grafted cellulose film obtained superior wettability to electrolyte compared with pure cellulose film [36]. However, the non-crosslinked AP swells infinitely when it was immersed in electrolyte with lithium salt. To further verify the infinite swelling of the non-crosslinked AP film, the electrolyte uptake capabilities was calculated by Eq. 1:

$$\lambda = \frac{(W_t - W_0) \times 100\%}{W_0} \quad (1)$$

where λ is the electrolyte uptake, W_0 is the weight of dry film, and W_t is the weight of the wet film after absorption of organic solvent. The non-crosslinked AP films were immersed in DMC/EC (1:1) liquid electrolytes either without a lithium salt or containing 1 mol/L LiTFSI. As shown in Fig. 1a, the films soaked in a mixed EC/DMC electrolyte reached equilibrium swelling within 1 h, with the electrolyte uptake of 87.8%. However, the films swelled rapidly within 30 min when it was soaked in the electrolyte containing the lithium salt LiTFSI. The illustration in Fig. 1a also demonstrated that the non-crosslinked AP film gradually increased from 10 min to 30 min. For the films soaked for 2 h, the electrolyte uptake increased to 959.4% until the structure of the membrane was completely destroyed, which suggests that the lithium salt may be the key factor affecting their structural stability.

To further characterize the stability of the Li metal anode/non-crosslinked AP GPE interface at different soaking time (10, 20 and 30 min), we assembled the symmetrical batteries with the non-crosslinked AP GPE sandwiched between two lithium foils to evaluate the lithium stripping/plating processes at a current density of 0.05 mA/cm^2 (Fig. 1b). For a 10-min AP GPE sample, the polarization voltage remained low and no short-circuit occurred even after cycling for over 1000 h. For 20-min and 30-min AP GPE samples, the overpotential increased rapidly during cycling. For the 30-min samples, a severe polarization of the battery, which ended with short-circuiting, started after 200 h of cycling. The inadequate stability of the interface between the Li metal anode and the 30-min AP GPE samples can be explained as follows: the structure of non-crosslinked AP GPE samples subjected to prolong soaking rapidly collapses, leading to persistent side reactions between the GPE and the lithium metal [16]. Meanwhile, the mechanical strength of 30 min AP GPE is inadequate to restrain the growth of lithium dendrites. Therefore, this result shows that the non-crosslinked AP GPEs subjected to prolong soaking in the considered liquid electrolytes cannot withstand prolong cycling.

To explore the mechanism of failure of non-crosslinked AP GPEs in the electrolytes containing the lithium salt, ^{7}Li NMR and ^{19}F NMR spectra were measured on an AVANCE NEO 400 spectrometer using dimethyl sulfoxide-d_6 as the solvent to identify the interaction between the AP film and LiTFSI salt. As shown in Fig. 1c, pure LiTFSI has a chemical shift at −1.038 ppm. This signal shifts slightly (to −1.017 ppm) after mixing with AP, which is extremely likely attributed to the complexation of Li^+ with the ether bonds in PEG, as shown in Fig. 1e [37,38]. Meanwhile, the ^{19}F-NMR spectrum in Fig. 1d conveys the interaction between the anion $TFSI^{-1}$ and AP polymer chains. The lithium salt LiTFSI has a single chemical shift of F proton at −78.73 ppm, and a new peak at −78.71 ppm appears in the ^{19}F-NMR spectrum after adding the salt to the AP solution. The new peak shown in Fig. 1f can be ascribed to the formation of hydrogen bonds between the $TFSI^{-1}$ anion and hydroxyl groups of the backbone of AP chains [39]. Collectively, the ^{7}Li-NMR and ^{19}F-NMR data suggest that the strong interaction between the lithium salt and the functional groups (ether linkages and hydroxyls) of AP can easily promote permeation of the liquid electrolyte into the structure of AP membrane, resulting in rapid swelling and subsequent destruction of the tangled structure.

In light of the findings above, we can state that crosslinking structure is an effective strategy to improve the mechanical properties and structural stability of non-crosslinked AP films. As displayed in Fig. 2a, the crosslinked AP was synthesized by thiol-ene click chemistry using UV-induced polymerization. The sol-gel states before and after crosslinking are shown in Fig. S1 (Support-

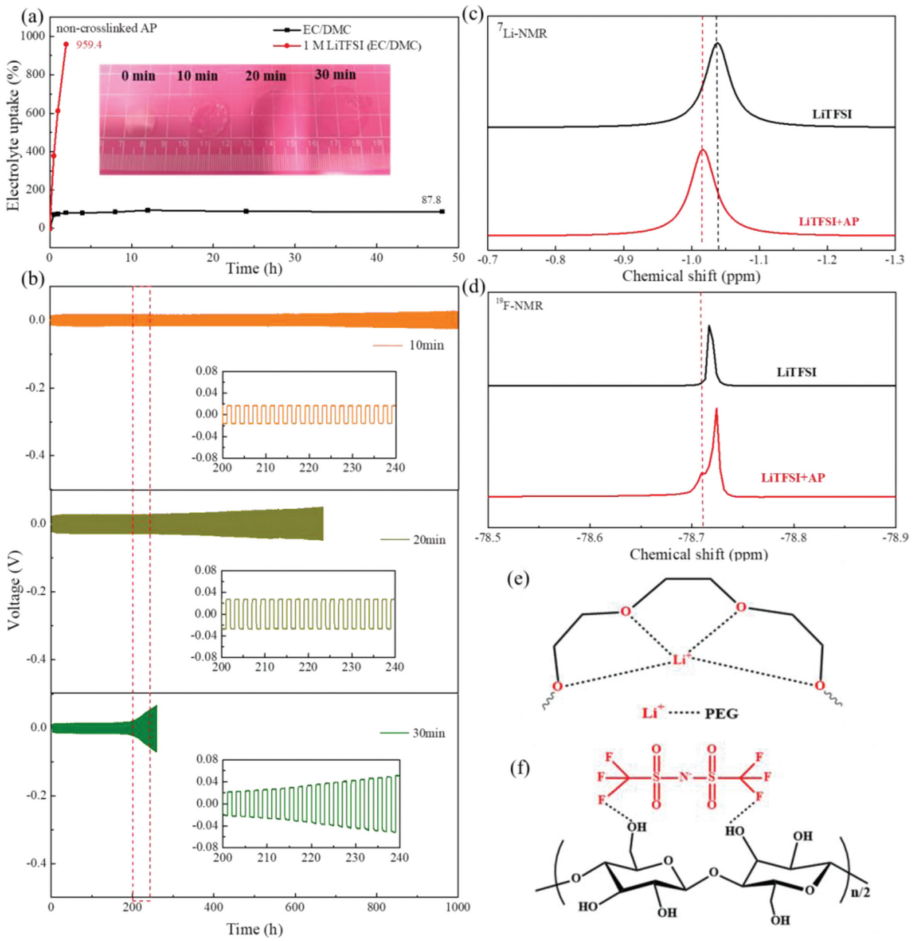

Fig. 1. (a) The electrolyte uptake of the non-crosslinked AP membrane soaked in EC/DMC and EC/DMC with 1 mol/L LiTFSI (DMC/EC = 1:1, v/v). The Inset: the state of the non-crosslinked AP film with different soaking time in the electrolyte (10, 20 and 30 min). (b) The voltage profiles of symmetric Li|Li cells based on the non-crosslinked AP GPE with different soaking time (10, 20 and 30 min) in the electrolyte at 0.05 mA/cm^2. (c) ^{7}Li-NMR of LiTFSI and the non-crosslinked AP with LiTFSI. (d) ^{19}F-NMR of LiTFSI and the non-crosslinked AP with LiTFSI. (e) the schematic diagram of the interaction mechanism of the ether bond and Li^+. (f) The schematic diagram of the interaction mechanism of the hydroxy and $TFSI^-$.

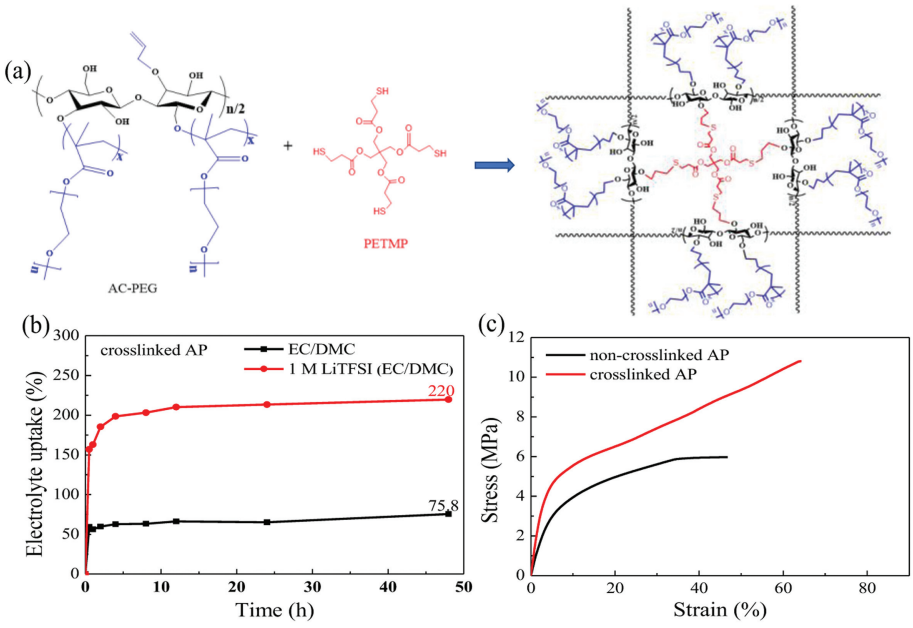

Fig. 2. (a) The synthesis mechanism of the crosslinked AP. (b) The electrolyte uptake of crosslinked AP soaked in EC/DMC and EC/DMC with 1 mol/L LiTFSI (DMC/EC = 1:1, v/v). (c) Stress-strain curves of non-crosslinked AP and crosslinked AP with a tensile rate of 0.1 N/min.

Table 1
The mechanical parameters of the non-crosslinked AP and the crosslinked AP.

Sample	Strain (%)	Tensile strength (MPa)	Tensile modulus (MPa)	Toughness (10^3 kJ/m^3)
Non-crosslinked AP	46.80	5.97	60.47	223.23
Crosslinked AP	64.73	10.95	114.78	483.56

ing information), the crosslinked AP is in a gel state and retains its shape even when inverted. The surface and cross-sectional morphology of the dry crosslinked AP film was studied using SEM with an accelerating voltage of 10 kV. As shown in Fig. S2 (Supporting information), the dried crosslinked AP films are homogeneous, and their porous structure can be observed from the cross-sectional SEM images. To test their structural integrity, the crosslinked AP films were immersed into EC/DMC and EC/DMC with 1 mol/L LiTFSI, respectively. As shown in Fig. 2b, the crosslinked AP films can reach equilibrium swelling in both electrolytes. Further, the crosslinked AP films displayed a much higher electrolyte uptake (up to 220%) in the lithium-containing solution than in the solution without lithium salt (75.8%). This result is consistent with the NMR data, *i.e.*, the presence of lithium salt promotes permeation of the AP films with the electrolyte and their subsequent swelling. As a result, the crosslinked AP film is able to retain the mechanical integrity of its structure while displaying the high electrolyte uptake, which is beneficial for the lithium-ion transport.

To verify this conclusion, we measured the mechanical properties of AP films before and after crosslinking at a loading rate of 0.1 N/min. Fig. 2c shows stress-strain curves for our AP films. For the non-crosslinked and crosslinked AP films, the tensile strength was 5.97 and 10.95 MPa, respectively, and the elongation was 46.8% and 64.73%, respectively. More detailed data on the mechanical properties are shown in Table 1. Crosslinked AP has a tensile modulus of 114.78 MPa and a toughness of 483.56×10^3 kJ/m^3, values nearly twice as high as those of its non-crosslinked counterpart. Apparently, the excellent mechanical properties of the crosslinked AP can be mainly credited to the internal crosslinking of its network and the rigid cellulose backbone. The observed mechanical properties decrease the risk of short-circuits inside the battery by suppressing the growth of lithium dendrites and improving the long-term cycling stability.

The thermal stability of the films was evaluated by thermogravimetric analysis (TGA) and differential scanning calorimetry (DSC) under N_2 atmosphere from 25 °C to 600 °C at a heating rate of 10 °C/min (Fig. S3 in Supporting information). As can be seen, the non-crosslinked AP and the crosslinked AP exhibited similar thermal stabilities, and both of them began to decompose at around 233 °C. Two heat absorption peaks in the DSC curve correspond to the decomposition of cellulose and PEGMA. Clearly, there is no significant difference between their thermal stability. The result shows that the low amount of added crosslinking agent (PETMP) has a negligible effect on thermal stability of the crosslinked and non-crosslinked AP.

It is well known that the strong electrolyte retention by GPEs is critical for safer operation of the battery due to lower leakage and volatilization of electrolyte. To investigate the film's ability to retain electrolyte, the non-crosslinked and crosslinked AP GPEs were stored at 25 and 60 °C, respectively. The results are shown in Fig. S4 (Supporting information). The mass of non-crosslinked 30-min AP GPEs stored at 25 °C changed only slightly, while the mass of sample kept at 60 °C was rapidly decreasing, so the weight retention after 48 h was only 52.7%. The mass of crosslinked AP GPEs kept at 25 or 60 °C for 48 h did not change significantly (weight retention 96.1% and 89.9%, respectively), which is indicative of the strong ability to retain electrolyte of the crosslinked AP.

The electrochemical window is evaluated by cyclic voltammetry (CV) in the voltage range of −0.5–5 V (*vs.* Li/Li) at a scan rate of 1 mV/s. As shown in Fig. S5 (Supporting information), non-crosslinked AP GPEs begin to degrade when the voltage rises to 4.65 V. In contrast, crosslinked AP GPEs displayed higher electrochemical stability (>5.0 V). This result shows that the crosslinked GPE can tolerate higher voltages and inhibit the oxidation reaction. Therefore, the crosslinked AP GPE exhibits better electrochemical stability, which suggests its potential application in high-voltage batteries.

Electrochemical impedance spectroscopy (EIS) is used to measure the stability of the interface between GPEs and lithium-metal electrodes, which is performed on the Biologic VSP-300 potentiostat in the range of response frequencies of 10^6–10^{-2} Hz at a voltage of 10 mV at 25 °C. EIS plots for symmetrical Li|Li batteries with non-crosslinked 30 min AP GPE and crosslinked AP GPEs are shown in Figs. 3a and b. The two semicircles at high and intermediate frequencies correspond to the passivation layer resistance (R_p) and charge transfer resistance (R_{ct}), respectively. The intercept at the real axis gives the bulk resistance (R_0). Initially, the impedance of Li|Li symmetrical batteries with non-crosslinked 30-min AP GPE was less than 100 Ω, but it rose dramatically within the following days. This can be due to the loose structure of the non-crosslinked AP after soaking in the electrolyte for 30 min and the fact that the AP matrix has poor electrolyte retention ability, which resulted in the continuous proceeding of the side reaction between the GPE and the lithium electrode. In contrast, the initial impedance of Li|Li symmetrical batteries with crosslinked AP GPEs was 375 Ω and it changed only slightly within the next few days, suggesting that the interface between the crosslinked AP GPE and the lithium electrode was sufficiently stable. Therefore, the crosslinked AP with a 3D network structure displays a strong solvent-blocking ability and superior stability of its interface with the metal anode.

The ionic conductivity has a direct impact on the electrochemical performance of GPEs, which is calculated according to Eq. 2:

$$\sigma = \frac{L}{R_b \cdot S} \tag{2}$$

here σ represents the ionic conductivity, S is the contact area between the GPE and the stainless steel disk, L is the thickness of GPE film, and R_b is the bulk ohmic resistance of a symmetrical battery described next. The temperature dependence of ionic conductivity for GPEs in the range of 25–55 °C is shown in Figs. 3c and d. SS/non-crosslinked AP GPEs/SS cells display a high ionic conductivity of 2.14×10^{-3} S/cm at 25 °C, while the crosslinked AP shows a slightly lower ionic conductivity of 1.57×10^{-3} S/cm. Meanwhile, the ionic conductivity was found to have a positive correlation with temperature, which is attributed to the faster motion of polymer chains and rapid migration of Li^+ at higher temperatures. The corresponding data are summarized in Table S1 (Supporting information). In addition, this result is consistent with the Arrhenius formula:

$$\sigma = \sigma_0 \exp\left(-\frac{E_a}{kT}\right) \tag{3}$$

where E_a refers to the activation energy, σ_0 is the pre-exponential factor, k is the Boltzmann constant (8.314×10^{-3} kJ mol^{-1} K^{-1}), and T is the temperature. The activation energy of crosslinked AP (19.1 kJ/mol) was calculated from the slope of the fitting line (Fig. 3f), which proved to be higher than the value for non-crosslinked AP GPEs (8.56 kJ/mol, Fig. 3e). This shows that the crosslinked network has a higher energy barrier to ion migration. This is why the ionic conductivity of crosslinked AP is lower than that of non-crosslinked AP at room temperature. But the higher activation energy of crosslinked AP makes itself more sensitive to changes in temperature. Small temperature changes can cause a

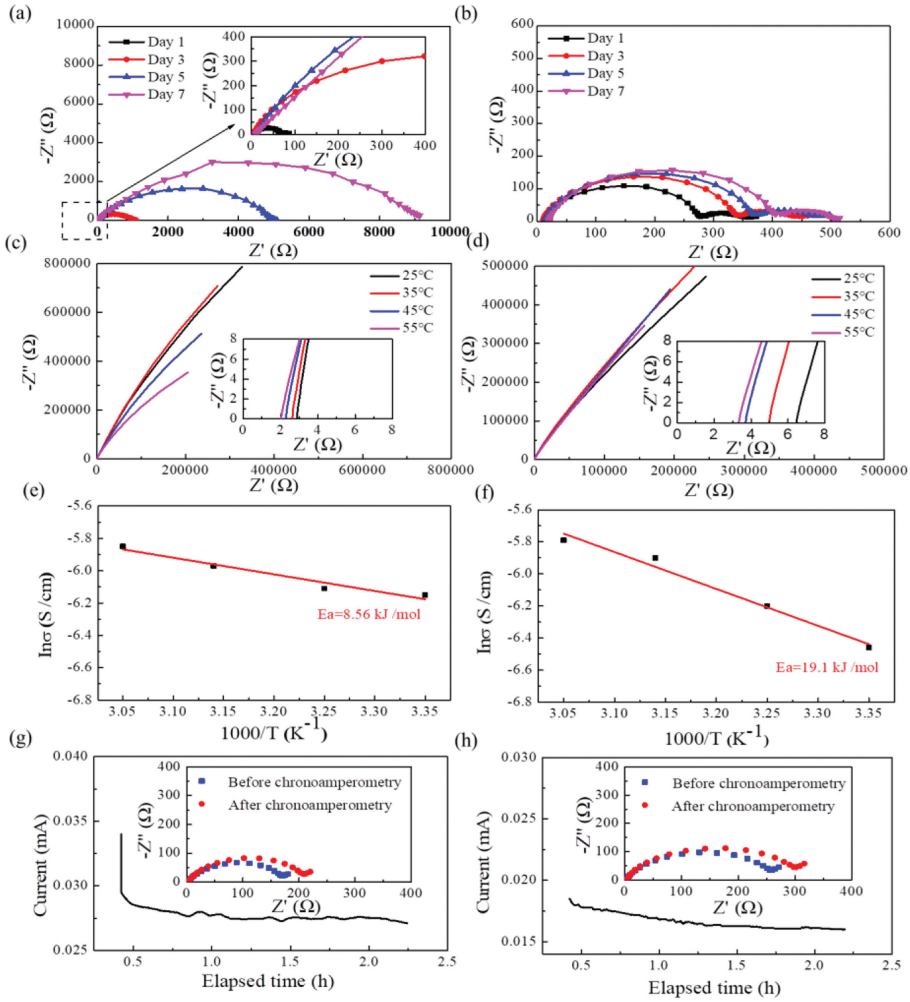

Fig. 3. EIS plots of Li|Li symmetrical batteries with non-crosslinked AP GPEs (a) and crosslinked AP GPEs (b) on days 1, 3, 5 and 7. Impedance plots of SS|SS symmetrical batteries with (c) non-crosslinked AP GPEs and (d) crosslinked AP GPEs in the range of 25–55 °C. The ionic conductivity Arrhenius fitting curves of (c) non-crosslinked AP GPEs and (f) crosslinked AP GPE at different temperatures. Chronoamperometry curves of Li|Li cells with (g) non-crosslinked AP GPEs and (h) crosslinked AP GPEs at the potential of 10 mV. Inset: electrochemical impedance spectroscopy (EIS) plots of the batteries before and after chronoamperometry measurements.

rapid rise in the ionic conductivity of crosslinked AP GPEs. The latter displays a higher ionic conductivity of 3.06×10^{-3} S/cm at 55 °C compared to non-crosslinked AP GPEs (2.88×10^{-3} S/cm).

The lithium-ion transference number (t_{Li^+}) is another important parameter of the GPEs. The symmetrical battery was assembled by placing the GPE between two lithium foils to measure lithium-ion transference number t_{Li^+} by chronoamperometry (CA) in combination with EIS (voltage of 10 mV, at room temperature) performed before and after CA measurement. The transference number was calculated from Eq. 4:

$$t_{Li^+} = \frac{I_S(U - R_0 I_0)}{I_0(U - R_S I_S)} \quad (4)$$

where U is the applied voltage (10 mV); I_0 and I_s refer to the initial and steady-state currents, respectively; R_0 and R_s are the initial and steady-state interfacial resistances of GPE electrodes before and after CA, respectively. With high t_{Li^+} values, the polarization is effectively lower, and the possibility of lithium dendrite growth is lower as well, which is important for practical application of the GPEs in lithium batteries [40]. As shown in Figs. 3g and h, both non-crosslinked and crosslinked APs display a high and essentially identical t_{Li^+} values, which are 0.81 and 0.79, respectively. The high t_{Li^+} values can be attributed to the strong hydrogen bonding between $TFSI^{-1}$ and the hydroxyl groups of the polymer matrix, which was verified by the ^{19}F-NMR spectrum presented above. The immobilization of anionic component of the lithium salt inside the polymer matrix helps to improve the single lithium-ion transport. In addition, the ether oxygen groups in PEG and glycosidic bonds of the cellulose chain can also contribute to the lithium-ion transport by providing a large number of channels for the movement of lithium ions. Therefore, the crosslinking process does not affect the lithium-ion transference number.

Due to the excellent electrochemical properties and structural stability of crosslinked AP GPEs, the Li|Li symmetrical batteries and $LiFePO_4$|Li batteries are assembled to test their cycling performance. First, the Li|Li symmetrical cells were tested at a current density of 0.1 mA/cm^2. As can be observed from Fig. S6 (Supporting information), the symmetrical cell with crosslinked AP GPEs delivered low polarization voltage (below 0.4 V) and long cycling stability (600 h). In contrast, the polarization voltage of symmetrical cell with non-crosslinked AP GPEs gradually increased after 200 h due to the structural instability and poor mechanical properties.

The cycle performance and rate capability of the $LiFePO_4$/GPEs/Li cells were measured on the LAND CT 2001A battery test system in the range of charge-discharge voltages of 2.5–4.2 V at 25 °C. $LiFePO_4$/Li coin cells were assembled in an Ar-filled glove box by placing the GPEs between the $LiFePO_4$ cathode and a lithium anode, and the areal mass loading of the LFP cathode was about 2.54 mg/cm^2.

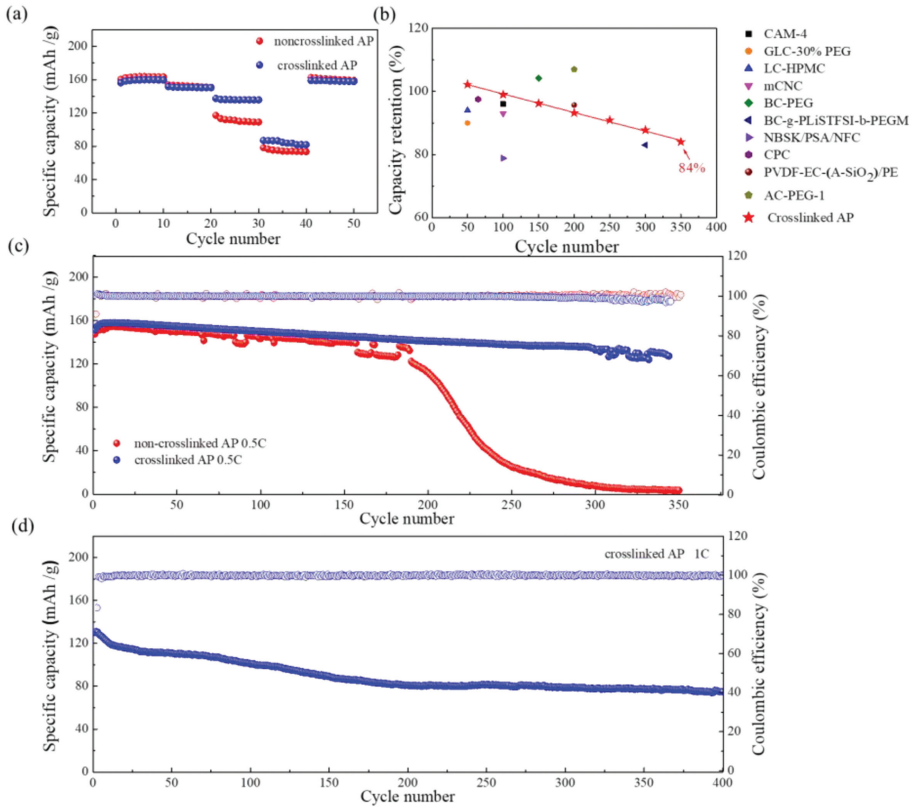

Fig. 4. (a) Rate performances of $LiFePO_4$|GPEs|Li batteries with non-crosslinked AP and crosslinked AP at 0.2, 0.5, 1.0 and 2 C. (b) Comparison of cycle life of $LiFePO_4$|GPEs|Li batteries with crosslinked AP and the reported cellulose-based GPEs at 0.5 C (CAM-4 [24], GLC-30% PEG [41], LC-HPMC [42], mCNC [43], BC-PEG [44], BC-g-PLiSTFSI-PEGM [45], NBSK/PSA/NFC [46], CPC [47], PVDF-EC-(A-SiO_2)/PE [48], AC-PEG-1 [36]). (c) Cycling performances of $LiFePO_4$|GPEs|Li batteries with non-crosslinked AP and crosslinked AP at 0.5 C. (d) Cycling performances of $LiFePO_4$|GPEs|Li batteries with crosslinked AP at 1 C.

The rate performance of $LiFePO_4$|Li cells with non-crosslinked AP GPEs and crosslinked AP GPEs from 0.2 C to 2 C is shown in Fig. 4a. The $LiFePO_4$|crosslinked AP GPEs |Li cell delivers reversible specific capacities of 159.8, 151.5, 136.3 and 86.8 mAh/g at 0.2, 0.5, 1 and 2 C, respectively. Moreover, when the current density was switched back to 0.2 C, there was almost no capacity attenuation, indicating that the Li-ion battery system based on crosslinked AP was highly stable. In contrast, the discharge capacity of $LiFePO_4$|GPEs|Li cell containing non-crosslinked AP is lower compared to its counterpart with crosslinked AP, especially at high current densities.

The long-term cycling performance at 0.5 C is shown in Fig. 4c, The $LiFePO_4$|crosslinked AP GPEs|Li cell delivers an initial discharge capacity of 151.5 mAh/g at 0.5 C, and displays the capacity retention of 84% after 350 cycles, which is superior to most of the reported cellulose-based GPEs. The comparison results are shown in Fig. 4b. Meanwhile, the structure of crosslinked AP GPEs after long cycles is relatively intact (Fig. S2c). But from the cross-section SEM images before and after long cycling (Fig. S2d), the film structure has been slightly destroyed and a few cellulose fibers escaped from the film. It demonstrated that the repeated charge-discharge process could gradually destroy the film's inner crosslinked structure and finally lead to the decay of battery's capacity. But the decay speed is much slower than that of non-crosslinked GPE. That's why the crosslinked AP could maintain high capacity retention after 350^{th} cycles while the non-crosslinked AP suffers from severe decay after 200^{th} cycles. What is more, as shown in Fig. 4d, the $LiFePO_4$|crosslinked AP|Li cell also has a stable charge and discharge process within 400 cycles at a higher current density of 1 C. Therefore, the crosslinked AP with good structural integrity and favorable mechanical properties is critical for long cycle life lithium-metal batteries.

In conclusion, a crosslinked cellulose-based gel polymer electrolyte was prepared *via* a simple and effective thiol-ene click reaction to address the issue of infinite swelling and structural instability of non-crosslinked AP in electrolyte solution. The prepared crosslinked AP features excellent electrochemical properties: high ionic conductivity at room temperature (1.57×10^{-3} S/cm) and a high ion transference number (0.79). Due to the favorable mechanical properties and resilient structure of our crosslinked AP, the $LiFePO_4$|Li batteries fabricated using the prepared material displayed good cyclic performance. The excellent performance of crosslinked AP prepared in this study may stimulate the use of crosslinked GPEs for creating highly safe and durable lithium-metal batteries.

Declaration of competing interest

The authors declare that they have no known competing financial interests or personal relationships that could have appeared to influence the work reported in this paper

Acknowledgments

This work is financially supported by National Natural Science Foundation of China (Nos. 21965012, 52003068, 52062012), Research Project of Hainan Province (Nos. ZDYF2021SHFZ263, 2019RC038 and ZDYF2020028), Guangdong Province Key Discipline Construction Project (No. 2021ZDJS102), the Innovation Team of Universities of Guangdong Province (No. 2022KCXTD030).

Supplementary materials

Supplementary material associated with this article can be found, in the online version, at doi:10.1016/j.cclet.2022.108031.

References

[1] W. Xu, J. Wang, F. Ding, et al., Energy Environ. Sci. 7 (2014) 513–537.
[2] D. Lin, Y. Liu, Y. Cui, Nat. Nanotechnol. 12 (2017) 194–206.
[3] F. Zheng, M. Kotobuki, S. Song, et al., J. Power Sources 389 (2018) 198–213.
[4] A. Manthiram, X. Yu, S. Wang, Nat. Rev. Mater. 2 (2017) 16103.
[5] Q. Pan, D.M. Smith, H. Qi, S. Wang, C.Y. Li, Adv. Mater. 27 (2015) 5995–6001.
[6] K. Deng, J. Qin, S. Wang, et al., Small (2018) e1801420.
[7] B. Liu, J.G. Zhang, W. Xu, Joule 2 (2018) 833–845.
[8] Y.M. Jeon, S. Kim, M. Lee, W.B. Lee, J.H. Park, Adv. Energy Mater. 10 (2020) 2003114.
[9] H. Fei, Y. Liu, Y. An, et al., J. Power Sources 399 (2018) 294–298.
[10] H.F. Fei, C.L. Wei, Y.C. Zhang, et al., Acta Phys. Chim. Sin. 36 (2020) 1905015.
[11] J. Li, F. Huo, T. Chen, et al., Energy Storage Mater. 40 (2021) 394–401.
[12] J. Li, Y. Cai, Y. Cui, et al., Nano Energy 95 (2022) 107027.
[13] J. Li, H. Zhang, Y. Cui, et al., Nano Energy 102 (2022) 107716.
[14] S. Tang, W. Guo, Y. Fu, Adv. Energy Mater. 11 (2020) 2000802.
[15] Z. Hu, G. Li, A. Wang, J. Luo, X. Liu, Batter. Supercaps 3 (2020) 331–335.
[16] Z. Li, X.Y. Zhou, X. Guo, Energy Storage Mater. 29 (2020) 149–155.
[17] S.H. Siyal, M. Li, H. Li, et al., Appl. Surf. Sci. 494 (2019) 1119–1126.
[18] L. Chen, Y. Li, S.P. Li, et al., Nano Energy 46 (2018) 176–184.
[19] H. Li, X.T. Ma, J.L. Shi, et al., Electrochim. Acta 56 (2011) 2641–2647.
[20] Z. Xue, D. He, X. Xie, J. Mater. Chem. A 3 (2015) 19218–19253.
[21] D. Golodnitsky, E. Strauss, E. Peled, S. Greenbaum, J. Electrochem. Soc. 162 (2015) A2551–A2566.
[22] Q. Lu, Y.B. He, Q. Yu, et al., Adv. Mater. 29 (2017) 1604460.
[23] W. Li, Y. Pang, J. Liu, et al., RSC Adv. 7 (2017) 23494–23501.
[24] J. Wan, J. Zhang, J. Yu, J. Zhang, ACS Appl. Mater. Interfaces 9 (2017) 24591–24599.
[25] X. Li, Y. Zheng, C.Y. Li, Energy Storage Mater. 29 (2020) 273–280.
[26] J. Zhang, S. Wang, D. Han, et al., Energy Storage Mater. 24 (2020) 579–587.
[27] W. Chen, H. Yu, S.Y. Lee, et al., Chem. Soc. Rev. 47 (2018) 2837–2872.
[28] X. Qiu, S. Hu, Materials 6 (2013) 738–781.
[29] Z. Wang, Y.H. Lee, S.W. Kim, et al., Adv. Mater. (2020) 2000892.
[30] E. Lizundia, C.M. Costa, R. Alves, S. Lanceros-Méndez, Carbohydr. Polym. Technol. Appl. 1 (2020) 100001.
[31] J.H. Kim, D. Lee, Y.H. Lee, W. Chen, S.Y. Lee, Adv. Mater. 31 (2019) e1804826.
[32] C. Yang, Q. Wu, W. Xie, et al., Nature 598 (2021) 590–596.
[33] S. Zhang, J. Luo, M. Du, F. Zhang, X. He, Cellulose (2022) 5163–5176.
[34] Y. Zhong, L. Zhong, S. Wang, et al., J. Mater. Chem. A 7 (2019) 24251–24261.
[35] Z. Du, Y. Su, Y. Qu, et al., Electrochim. Acta 299 (2019) 19–26.
[36] H. Zhang, S. Wang, A. Wang, et al., Appl. Surf. Sci. (2022) 153411.
[37] M. Shamsipur, M. Irandoust, Polyhedron 31 (2012) 395–401.
[38] M.J. Reddy, P.P. Chu, J. Power Sources 135 (2004) 1–8.
[39] F. Yu, H. Zhang, L. Zhao, et al., Carbohydr. Polym. 246 (2020) 116622.
[40] X. Guan, Q. Wu, X. Zhang, et al., Chem. Eng. J. 382 (2020) 122832.
[41] A. Song, Y. Huang, B. Liu, et al., Electrochim. Acta 247 (2017) 505–515.
[42] C. Luo, Y. Huang, Z. Yin, et al., Mater. Chem. Phys. 250 (2020) 123174.
[43] C. Hänsel, E. Lizundia, D. Kundu, A.C.S. Appl. Energy Mater. 2 (2019) 5686–5691.
[44] D. Xu, B. Wang, Q. Wang, et al., ACS Appl. Mater. Interfaces 10 (2018) 17809–17819.
[45] M. Zhou, R. Liu, D. Jia, et al., Adv. Mater. 33 (2021) e2100943.
[46] H. Zhang, J. Liu, M. Guan, et al., ACS Sustain. Chem. Eng. 6 (2018) 4838–4844.
[47] R. Pan, X. Xu, R. Sun, et al., Small 14 (2018) e1704371.
[48] X. Zuo, J. Wu, X. Ma, et al., J. Power Sources 407 (2018) 44–52.